# Operator-sum models of quantum decoherence in molecular quantum-dot cellular automata

Jackson S. Ramsey and Enrique P. Blair[a)]
*Electrical and Computer Engineering Department, Baylor University, One Bear Place # 97356, Waco, Texas 76798, USA*

(Received 13 May 2017; accepted 28 June 2017; published online 28 August 2017)

Quantum-dot cellular automata is a paradigm for classical computing which departs from the transistor paradigm and provides a system in which quantum phenomena may be studied. Here, the elementary computing device is a cell, a structure having multiple quantum dots and a few mobile charges. A specific operator-sum representation is developed for an exactly modeled double-dot, molecular cell within an environment of $N$ similar neighboring molecules. While an operator-sum representation is not unique, a specific model can be determined by selecting a particular environmental basis. We select the environment's computational basis and calculate the specific and full set of $2^N$ Kraus operators, which match exactly previous models of quantum decoherence in this system. Finally, the timescale for environmental interaction is characterized, enabling the reduction of the large set of Kraus operators to an approximate pair of Kraus operators, exact in the limit of large $N$. *Published by AIP Publishing.* [http://dx.doi.org/10.1063/1.4993450]

## I. INTRODUCTION

Driven by system-environment interactions, quantum decoherence is a ubiquitous and powerful phenomenon. The loss of quantum coherence from systems plays an important role in the emergence of the classical world from the quantum substrate.[1] Disruptive in quantum computing systems, decoherence has been found to stabilize bits in molecular devices[2] within a general-purpose, classical computing paradigm known as quantum-dot cellular automata (QCA).[3,4]

Designed for low-power, energy-efficient computing beyond the transistor era, QCA provide an illuminating framework for the exploration of quantum mechanical phenomena. Here, we focus on quantum decoherence in molecular QCA. Section II provides a brief description of quantum-dot cellular automata, along with a discussion of the operator-sum representation. Section III describes models for a target double-dot molecule (the open quantum system of interest) in the center of an environment comprised of several similar molecules. First, an exact model is outlined for the unitary evolution of both the target molecule and environment treated explicitly as one composite system. A reduced density operator is traced out for a description of the target molecule. This was developed into a reduced but exact expression for time dynamics of the coherence vector for the target system only.[2] Next, we calculate for the same system a particular equivalent set of Kraus operators to obtain a reduced-dynamics operator-sum equation for the target molecule's reduced density matrix. This set of operators is very large: there is one Kraus operator for each of the numerous environmental degrees of freedom. Section IV shows the exact agreement between the operator-sum model and the direct coherence vector calculation. In the limit where the environmental effects dominate the system's internal dynamics, the principal system's coherence has a Gaussian decay. From the data shown, a direct relationship is found between the strength of the environmental interaction and the timescale of the Gaussian decay. This leads to a pair of Kraus operators, which approximate the full set in the limit of large environment population $N$.

## II. BACKGROUND

### A. Quantum-dot cellular automata (QCA)

In QCA, the elementary device is a system of quantum dots called a "cell." The configuration of mobile charge on the cell encodes a classical bit, and the intracellular, inter-dot quantum tunneling of the mobile charge enables device switching. Neighboring cells interact via the Coulomb field, enabling general-purpose computing. Specific arrangements of cells can function as QCA logic circuits.[3–5]

QCA may be implemented in several ways. Photolithography was used to fabricate the earliest cells with metal islands providing quantum dots on an insulating surface.[6–13] QCA cells also have been fabricated with semiconductor dots.[14,15] Arrangements of cells have been "written" on silicon surfaces using a scanning-tunneling microscope tip.[16] QCA also may be implemented using mixed-valence molecules, in which molecules function as cells and redox centers on a molecule provide dots.[17–20] QCA molecules offer advantages such as synthetic regularity between cells, ultra-high device densities, room-temperature operation, and high operating speeds limited by pico-second-or-faster electron transfer times. The molecular implementation is the focus here. In this implementation, a molecule typically functions as a cell, so the terms "molecule" and "cell" are used interchangeably throughout this discussion.

### B. The operator-sum representation

The operator-sum representation is a method for modeling non-unitary effects of an external system $\mathcal{E}$ on the density

[a)]Electronic mail: Enrique_Blair@baylor.edu

matrix $\hat{\rho}_{\mathcal{S}}$ of a principal open quantum system $\mathcal{S}$ ($\mathcal{E}$ usually is a measurement apparatus or the environment).[21] An operator-sum representation avoids the explicit treatment of the degrees of freedom of $\mathcal{E}$, transforming $\hat{\rho}_{\mathcal{S}}$ using a set of Kraus operators which act only on the Hilbert space of $\mathcal{S}$. These Kraus operators, then, must contain information about $\mathcal{E}$ and its impact on the open system $\mathcal{S}$. The operator-sum representation is useful when the details of $\mathcal{E}$ are not fully known, or when $\mathcal{E}$ is large and it is undesirable to model its degrees of freedom. Such methods that avoid an explicit treatment of $\mathcal{E}$ are referred to as "reduced dynamics" models.

Among reduced dynamics models, the operator-sum representation is very general. For example, the Lindblad equation assumes that $\mathcal{E}$ is Markovian or memoryless,[22] restricting the set of behaviors a Lindblad-based model can capture. The operator-sum representation, however, can model the effects of a non-Markovian $\mathcal{E}$ on $\mathcal{S}$.

The operator-sum representation was chosen for this study because previous work revealed dynamics in the system of interest reflective of a non-Markovian environment.[2] Starting with the quantum Liouville equation, Appendix A provides a derivation of the operator-sum representation, as well as an outline of the calculation of the individual Kraus operators which specify the operator-sum representation for this system.

## III. MODELS

### A. Full system + environment model

The system of interest, $\mathcal{S}$, is a double-dot molecule with two quantum dots separated by distance $a$. One mobile electron may tunnel between the dots with hopping energy $\gamma_{\mathcal{S}}$. The dots are treated as point charges, and the fully localized electronic states $\mathcal{B} = \{|0_{\mathcal{S}}\rangle, |1_{\mathcal{S}}\rangle\}$ are shown in Fig. 1. Not pictured here is the fixed, neutralizing charge, which is built into the model to reflect the fact that the molecules have a net zero charge. This neutralizing charge is located on and split evenly between the pair of quantum dots.

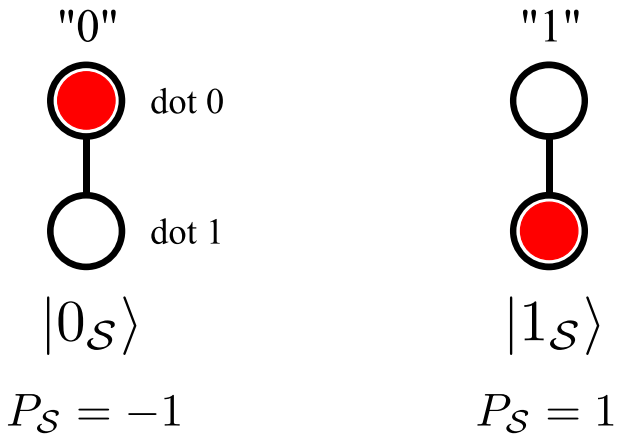


FIG. 1. Localized electronic states of the target molecular system. The electronic configuration of mobile charge on a mixed-valence molecule is shown here with one mobile electron (red disc) and two redox centers functioning as quantum dots (black circles). A tunneling path is denoted by a line connecting the two dots. The two localized electronic states are labeled $|0_{\mathcal{S}}\rangle$ and $|1_{\mathcal{S}}\rangle$ and form the computational basis for the system. The electronic configuration is quantified using a polarization $P_{\mathcal{S}} \in [-1, 1]$.

The Hamiltonian $\hat{H}_{\mathcal{S}}$ for the unperturbed target molecule $\mathcal{S}$ is given by

$$\hat{H}_{\mathcal{S}} = -\gamma_{\mathcal{S}}\hat{\sigma}_1 .$$

Here, $\hat{H}_{\mathcal{S}}$ is proportional to $\hat{\sigma}_1$, the first of the Pauli matrices

$$\begin{aligned}\hat{\sigma}_1 &= |0_{\mathcal{S}}\rangle\langle 1_{\mathcal{S}}| + |1_{\mathcal{S}}\rangle\langle 0_{\mathcal{S}}| \\ \hat{\sigma}_2 &= i(|0_{\mathcal{S}}\rangle\langle 1_{\mathcal{S}}| - |1_{\mathcal{S}}\rangle\langle 0_{\mathcal{S}}|) \\ \hat{\sigma}_3 &= -|0_{\mathcal{S}}\rangle\langle 0_{\mathcal{S}}| + |1_{\mathcal{S}}\rangle\langle 1_{\mathcal{S}}| .\end{aligned}$$

To provide environmental quantum degrees of freedom with which the system $\mathcal{S}$ can entangle, an environment $\mathcal{E}$ comprised of $N$ molecules similar to the target molecule $\mathcal{S}$ is established. The molecules of $\mathcal{E}$ are placed randomly on the surface of a sphere of radius $R$ centered on the target molecule. Additionally, the orientations of the environmental molecules are randomized, as shown in Fig. 2. It should be noted that the environmental molecules do not provide molecular logic but simply provide quantum degrees of freedom with which the target cell can entangle.

A convenient basis for the environment is the computational basis for $N$ two-state molecules

$$\begin{aligned}|\vec{m}_p\rangle &= |m_N m_{N-1} \cdots m_2 m_1\rangle \\ &\equiv |m_N\rangle|m_{N-1}\rangle \cdots |m_2\rangle|m_1\rangle ,\end{aligned} \tag{1}$$

where $m_k \in \{0, 1\}$, with the positive integer $k$ labeling an environment cell. Here, $\{|0_k\rangle, |1_k\rangle\}$ are the localized electronic states of the $k$th cell. Thus, $\vec{m}_p$ is an $N$-bit binary word,

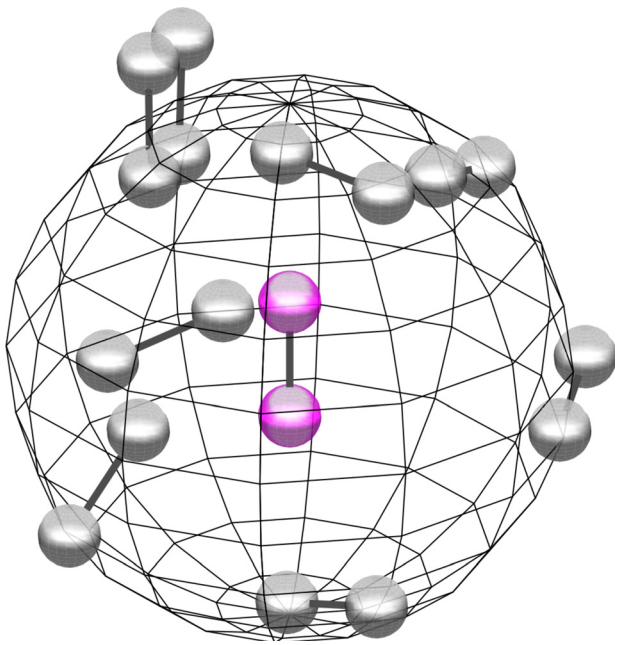

FIG. 2. A target cell with a simple environment. Here, a target QCA molecule is at the center of an environmental sphere comprised of $N = 8$ environmental molecules. All molecules are modeled as two quantum dots separated by a distance $a = 1$ nm. Two purple spheres represent the quantum dots of the target molecule, and gray spheres represent the quantum dots of environmental molecules. Paired dots are connected by a dark-gray bar, indicating a tunneling path. The environmental shell has a radius $R = 2.25a$.

and the non-negative integer $p \in \{0, 1, 2, \ldots, N_{\mathcal{E}} - 1\}$ indexes one of the $N_{\mathcal{E}} = 2^N$ environmental basis states.

The set of states $\{|\vec{m}_q\rangle = |\vec{m}_p\rangle|m_0\rangle\}$ form a global computational basis set for the system + environment composite system. Here, $m_0 \in \{0_{\mathcal{S}}, 1_{\mathcal{S}}\}$ is a label for a basis state of $\mathcal{S}$. Also, $\vec{m}_q$ is the $(N+1)$-bit binary word $\vec{m}_p m_0 = m_N m_{N-1} \cdots m_2 m_1 m_0$, and $q \in \{0, 1, \ldots, 2N_{\mathcal{E}} - 1\}$ is a non-negative integer indexing the global basis states.

We write the global Hamiltonian as

$$\hat{H} = \hat{H}_{\mathcal{S}} + \hat{H}_{\mathcal{E}} + \hat{H}_{\mathcal{SE}} \,. \tag{2}$$

The second term, $\hat{H}_{\mathcal{E}}$, includes all the Coulomb energy of interaction between all environmental cells as well as hopping energies for each cell in $\mathcal{E}$. The third term, $\hat{H}_{\mathcal{SE}}$, is a diagonal matrix in the computational basis, in which each element $\langle \vec{m}_q | \hat{H}_{\mathcal{SE}} | \vec{m}_q \rangle$ is the Coulomb energy of interaction between the system in state $|m_0\rangle$ and the environment in state $|\vec{m}_p\rangle$.

Most generally, the coherent evolution of the global system is described in density matrix formalism by the quantum Liouville equation

$$\frac{d}{dt}\hat{\rho} = -\frac{i}{\hbar}\left[\hat{H}, \hat{\rho}\right], \tag{3}$$

with solution

$$\hat{\rho}(t) = \hat{U}(t)\hat{\rho}(0)\hat{U}^{\dagger}(t) \,. \tag{4}$$

Here, $\hat{\rho}(t)$ is the time-dependent global density matrix with initial state $\hat{\rho}(0)$, and $\hat{U}(t)$ is the time evolution operator

$$\hat{U}(t) = \exp\left(-\frac{i}{\hbar}\hat{H}t\right). \tag{5}$$

A reduced density matrix $\hat{\rho}_{\mathcal{S}}^{(r)}(t)$ for the system of interest $\mathcal{S}$ may be found by tracing $\hat{\rho}(t)$ over the environmental degrees of freedom

$$\hat{\rho}_{\mathcal{S}}^{(r)}(t) = \mathrm{Tr}_{\mathcal{E}}\hat{\rho}(t) \equiv \sum_{j_{\mathcal{E}}} \langle j_{\mathcal{E}} | \hat{\rho}(t) | j_{\mathcal{E}} \rangle \,. \tag{6}$$

Here, $\{|j_{\mathcal{E}}\rangle\}$ is any orthonormal basis for the environment $\mathcal{E}$. We henceforth omit the superscript $(r)$ denoting a reduced density matrix.

Because $\mathcal{S}$ is a two-state system, the real degrees of freedom of $\hat{\rho}_{\mathcal{S}}$ are captured in the components of a three-element coherence vector $\vec{\lambda}^{\mathcal{S}} = (\lambda_1^{\mathcal{S}}, \lambda_2^{\mathcal{S}}, \lambda_3^{\mathcal{S}})$

$$\begin{aligned}\hat{\rho}_{\mathcal{S}} &= \frac{1}{2}\left(\hat{I} + \lambda_1^{\mathcal{S}}\begin{bmatrix} 0 & 1 \\ 1 & 0 \end{bmatrix} + \lambda_2^{\mathcal{S}}\begin{bmatrix} 0 & 1 \\ -i & 0 \end{bmatrix} + \lambda_3^{\mathcal{S}}\begin{bmatrix} 1 & 0 \\ 0 & -1 \end{bmatrix}\right) \\ &= \frac{1}{2}\left(\hat{I} + \lambda_1^{\mathcal{S}}\hat{\sigma}_1 + \lambda_2^{\mathcal{S}}\hat{\sigma}_2 + \lambda_3^{\mathcal{S}}\hat{\sigma}_3\right).\end{aligned} \tag{7}$$

Here, $\hat{\sigma}_1$, $\hat{\sigma}_2$, and $\hat{\sigma}_3$ are the Pauli matrices. The components of $\vec{\lambda}^{\mathcal{S}}$ are given by

$$\lambda_{\alpha}^{\mathcal{S}} = \mathrm{Tr}(\hat{\sigma}_{\alpha}\hat{\rho}_{\mathcal{S}}), \quad \alpha \in \{1, 2, 3\}. \tag{8}$$

The length of the coherence vector, $|\vec{\lambda}^{\mathcal{S}}|$, is a measure of coherence. A coherence vector of unit length is fully coherent, whereas coherence vectors of decreasing length have increasing decoherence.[23]

For the two-dot molecules in this model, a classical bit is encoded in the sign of the polarization $P$, which is the expectation value of $\hat{\sigma}_3$, or, equivalently, the value of $\lambda_3$

$$P = \langle \hat{\sigma}_3 \rangle = \lambda_3 \,. \tag{9}$$

To prevent dissipative effects from complicating the model dynamics, the transfer of energy between $\mathcal{S}$ and $\mathcal{E}$ is eliminated by fixing the charge configuration of the cells in $\mathcal{E}$. This is achieved by setting the tunneling energy for the environment cells equal to zero ($\gamma_{\mathcal{E}} = 0$). We refer to this as the non-dissipative limit.

### B. A reduced calculation of target cell dynamics in the non-dissipative limit

Within the non-dissipative limit, an exact, semi-analytic reduced model for target cell dynamics was obtained without numerically evaluating Eqs. (4) and (6). In this reduced model, the time evolution of the target cell's coherence vector from initial state $\vec{\lambda}^{\mathcal{S}}(0) = (\lambda_1^{\mathcal{S}}(0), \lambda_2^{\mathcal{S}}(0), \lambda_3^{\mathcal{S}}(0))$ is given by

$$\begin{aligned}\lambda_1^{\mathcal{S}}(t) &= \frac{\lambda_1^{\mathcal{S}}(0)}{N_{\mathcal{E}}}\sum_{p=0}^{N_{\mathcal{E}}-1}\frac{4\gamma_{\mathcal{S}}^2 + \left(E_{\vec{m}_p}^{\mathrm{flip}}\right)^2 \cos\left(\frac{\epsilon_{\vec{m}_p}}{\hbar}t\right)}{\epsilon_{\vec{m}_p}^2}, \\ \lambda_2^{\mathcal{S}}(t) &= \frac{\lambda_2^{\mathcal{S}}(0)}{N_{\mathcal{E}}}\sum_{p=0}^{N_{\mathcal{E}}-1}\cos\left(\frac{\epsilon_{\vec{m}_p}}{\hbar}t\right) \\ &\quad + \frac{\lambda_3^{\mathcal{S}}(0)}{N_{\mathcal{E}}}\sum_{p=0}^{N_{\mathcal{E}}-1}\frac{2\gamma_{\mathcal{S}}}{\epsilon_{\vec{m}_p}}\sin\left(\frac{\epsilon_{\vec{m}_p}}{\hbar}t\right), \text{ and} \\ \lambda_3^{\mathcal{S}}(t) &= -\frac{\lambda_2^{\mathcal{S}}(0)}{N_{\mathcal{E}}}\sum_{p=0}^{N_{\mathcal{E}}-1}\frac{2\gamma_{\mathcal{S}}}{\epsilon_{\vec{m}_p}}\sin\left(\frac{\epsilon_{\vec{m}_p}}{\hbar}t\right) \\ &\quad + \frac{\lambda_3^{\mathcal{S}}(0)}{N_{\mathcal{E}}}\sum_{p=0}^{N_{\mathcal{E}}-1}\frac{4\gamma_{\mathcal{S}}^2\cos\left(\frac{\epsilon_{\vec{m}_p}}{\hbar}t\right) + \left(E_{\vec{m}_p}^{\mathrm{flip}}\right)^2}{\epsilon_{\vec{m}_p}^2},\end{aligned} \tag{10}$$

where

$$\epsilon_{\vec{m}_p} = \sqrt{4\gamma_{\mathcal{S}}^2 + \left(E_{\vec{m}_p}^{\mathrm{flip}}\right)^2} \,. \tag{11}$$

Here, $E_{\vec{m}_p}^{\mathrm{flip}}$ is the detuning between the $|0_{\mathcal{S}}\rangle$ and $|1_{\mathcal{S}}\rangle$ states given a particular environment state $|\vec{m}_p\rangle$, or equivalently, $E_{\vec{m}_p}^{\mathrm{flip}}$ is the energy of a bit flip in the target cell from $|0_{\mathcal{S}}\rangle$ to $|1_{\mathcal{S}}\rangle$ when the environment is in state $|\vec{m}_p\rangle$:

$$E_{\vec{m}_p}^{\mathrm{flip}} = \langle \vec{m}_p 1_{\mathcal{S}} | \hat{H} | \vec{m}_p 1_{\mathcal{S}} \rangle - \langle \vec{m}_p 0_{\mathcal{S}} | \hat{H} | \vec{m}_p 0_{\mathcal{S}} \rangle \,. \tag{12}$$

The internal dynamics of $\mathcal{S}$ are captured by $\gamma_{\mathcal{S}}$, and decoherence is driven by environmental interaction, captured in the set of bit flip energies $E_{\vec{m}_p}^{\mathrm{flip}}$. The model of Eq. (10) was shown to be equivalent to the full, explicit model of Sec. III A in the non-dissipative limit.[2]

### C. An operator-sum model for non-dissipative target cell dynamics

An operator-sum model was derived without approximation from the full, explicit treatment of the $\mathcal{S}+\mathcal{E}$ composite system (see Sec. III A) in the non-dissipative limit. The equation for an operator-sum representation is

$$\hat{\rho}_{\mathcal{S}}(t) = \sum_{p=0}^{N_{\mathcal{E}}-1} \hat{K}_{\vec{m}_p}(t)\hat{\rho}_{\mathcal{S}}(0)\hat{K}^{\dagger}_{\vec{m}_p}(t), \tag{13}$$

in which the effects of the environment are modeled by the $N_{\mathcal{E}}$ Kraus operators $\{\hat{K}_{\vec{m}_p}(t)\}$, each of which acts on the Hilbert space of $\mathcal{S}$. For this model, the $p$th Kraus operator is given by

$$\hat{K}_{\vec{m}_p}(t) = \frac{1}{\epsilon_{\vec{m}_p}}\frac{1}{\sqrt{N_{\mathcal{E}}}}\left(\epsilon_{\vec{m}_p}\cos\left(\frac{\epsilon_{\vec{m}_p}t}{2\hbar}\right)\hat{I} + i\sin\left(\frac{\epsilon_{\vec{m}_p}t}{2\hbar}\right)\left(2\gamma_{\mathcal{S}}\hat{\sigma}_1 + E^{\text{flip}}_{\vec{m}_p}\hat{\sigma}_3\right)\right). \tag{14}$$

Appendix A provides an outline of the derivation of this result.

To focus on decoherence alone, we consider the limit in which environmental interaction dominates the internal dynamics of $\mathcal{S}$ ($\gamma_{\mathcal{S}} \to 0$). In this case, $\epsilon_{\vec{m}_p}$ reduces to $|E^{\text{flip}}_{\vec{m}_p}|$, and the time-dependent target cell coherence vector of Eq. (10) reduces to

$$\begin{aligned} \lambda^{\mathcal{S}}_1(t) &= \lambda^{\mathcal{S}}_1(0)f(t), \\ \lambda^{\mathcal{S}}_2(t) &= \lambda^{\mathcal{S}}_2(0)f(t), \quad \text{and} \\ \lambda^{\mathcal{S}}_3(t) &= \lambda^{\mathcal{S}}_3(0), \end{aligned} \tag{15}$$

where

$$f(t) = \frac{1}{N_{\mathcal{E}}}\sum_{p=0}^{N_{\mathcal{E}}-1}\cos\left(\frac{|E^{\text{flip}}_{\vec{m}_p}|}{\hbar}t\right). \tag{16}$$

Also, the $p$th Kraus operator of Eq. (14) reduces to

$$\hat{K}_{\vec{m}_p}(t) = \frac{1}{\sqrt{N_{\mathcal{E}}}}\left(\cos\left(\frac{|E^{\text{flip}}_{\vec{m}_p}|t}{2\hbar}\right)\hat{I} + i\frac{E^{\text{flip}}_{\vec{m}_p}}{|E^{\text{flip}}_{\vec{m}_p}|}\sin\left(\frac{|E^{\text{flip}}_{\vec{m}_p}|t}{2\hbar}\right)\hat{\sigma}_3\right). \tag{17}$$

## IV. RESULTS

The results of the reduced dynamics models from Sec. III—all within the non-dissipative limit ($\gamma_{\mathcal{E}} = 0$)—are presented here. Section IV A shows the operator-sum representation equivalent to the direct coherence vector calculation in the general case of decoherence and significant internal system dynamics ($\gamma_{\mathcal{S}} \neq 0$). Then, in Sec. IV B, the operator-sum model is shown to drive a Gaussian decoherence in $\mathcal{S}$ when the internal dynamics of $\mathcal{S}$ are dominated by environmental decoherence ($\gamma_{\mathcal{S}} \to 0$). The timescale for this Gaussian decoherence is related directly to the strength of the environmental interaction. Finally, in Sec. IV C, the full set of Kraus operators is reduced to a pair of Kraus operators in the limit of $\gamma_{\mathcal{S}} \to 0$. This reduction yields an approximate model, which becomes exact in the limit $N \to \infty$.

### A. Operator-sum representation: Decoherence with system internal dynamics

The operator-sum model agrees exactly with direct coherence vector calculation of Eq. (10), which was shown to agree exactly with the full model of Sec. III A in the non-dissipative limit.[2] Figure 3 shows the agreement between these two reduced models. Shown here is an example of the more general case in which dynamics internal to the target molecule $\mathcal{S}$ are significant relative to the environmentally driven decoherence ($\gamma_{\mathcal{S}} \neq 0$). Thus, a suitable timescale here is the Rabi oscillation period $\tau = \pi\hbar/\gamma_{\mathcal{S}}$ of the unperturbed target molecule.

Figure 4 shows the evolution of coherence for the same calculation as measured by the length $|\vec{\lambda}^{\mathcal{S}}(t)|$ of the coherence vector $\vec{\lambda}^{\mathcal{S}}(t)$. The $|\vec{\lambda}^{\mathcal{S}}(t)|$ calculation is performed for the same time evolution as shown in Fig. 3. Two competing effects are observed here: environmentally driven decoherence reduces $|\vec{\lambda}^{\mathcal{S}}(t)|$ from its initial value, but dynamics internal to the target cell $\mathcal{S}$ cause coherent oscillations in $\vec{\lambda}^{\mathcal{S}}(t)$, and thus in $|\vec{\lambda}^{\mathcal{S}}(t)|$.[2]

### B. Operator-sum representation: Decoherence dominates system internal dynamics

Next, we restrict the problem to the limit in which the internal cellular dynamics of $\mathcal{S}$ are dominated by environmentally driven decoherence ($\gamma_{\mathcal{S}} \to 0$). In this limit, the target cell's polarization $P(t) = \lambda^{\mathcal{S}}_3(t)$ is fixed because the inter-dot tunneling of charge within $\mathcal{S}$ is suppressed. Thus, the decay in $|\vec{\lambda}^{\mathcal{S}}(t)|$ is due entirely to $\lambda^{\mathcal{S}}_1(t)$ and $\lambda^{\mathcal{S}}_2(t)$, which

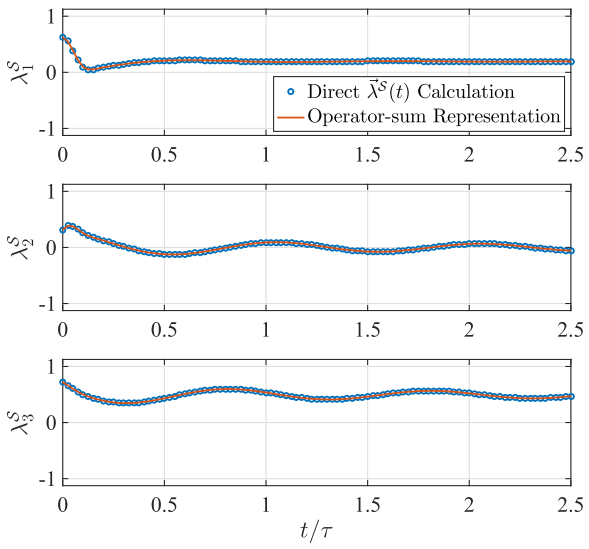


FIG. 3. Exactly the same time dependence is calculated for the target cell's coherence vector $\vec{\lambda}$ using two distinct methods: (a) the direct $\vec{\lambda}^{\mathcal{S}}(t)$ calculation of Eq. (10), and (b) the full operator-sum model of the target cell's time evolution given by Eqs. (13) and (14). Here, cells with $a = 1$ nm are used. The target cell has hopping energy $\gamma_{\mathcal{S}} = 100$ meV. The environmental shell has a population of $N = 18$ molecules and a radius of $R = 1.75a$.

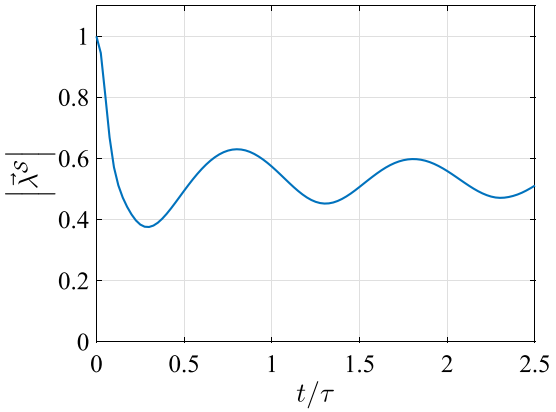


FIG. 4. The time dependence of quantum coherence as measured by the length $|\vec{\lambda}^{\mathcal{S}}(t)|$ of the coherence vector $\vec{\lambda}^{\mathcal{S}}(t)$. Here, $|\vec{\lambda}^{\mathcal{S}}(t)|$ corresponds to the $\vec{\lambda}^{\mathcal{S}}(t)$ shown in Fig. 3. Initially, for $t \lesssim 0.25\tau$, coherence decays rapidly from full coherence ($|\vec{\lambda}^{\mathcal{S}}(0)| = 1$) to a partial coherence. After the initial rapid decay ($t \gtrsim 0.25\tau$), coherent oscillations in $\vec{\lambda}^{\mathcal{S}}(t)$ and $|\vec{\lambda}^{\mathcal{S}}(t)|$ persist because of internal dynamics of the system $\mathcal{S}$.

depend on $f(t)$ per Eq. (15). A plot of $\vec{\lambda}^{\mathcal{S}}(t)$ is given in Fig. 5. Here, the timescale $\tau_{\mathcal{E}}$ is chosen as

$$\tau_{\mathcal{E}} = \frac{\pi\hbar}{E_o}, \tag{18}$$

where $E_o$ is the root-mean-square value of the detuning energy $E^{\text{flip}}_{\vec{m}_p}$ over all environmental basis states $|\vec{m}_p\rangle$.

For the evolution of Fig. 5, the loss of system coherence as quantified by $|\vec{\lambda}^{\mathcal{S}}(t)|$ is shown in Fig. 6. Since the value of $\lambda_3^{\mathcal{S}}(t)$ is fixed at $\lambda_3^{\mathcal{S}}(0)$, this establishes a hard minimum value for coherence: $|\vec{\lambda}^{\mathcal{S}}(t)| \geq |\lambda_3^{\mathcal{S}}(0)|$. The loss of coherence here is driven by the environmental interaction, which dominates any coherent oscillations in $\vec{\lambda}^{\mathcal{S}}(t)$. The absolute value $|f|$ of

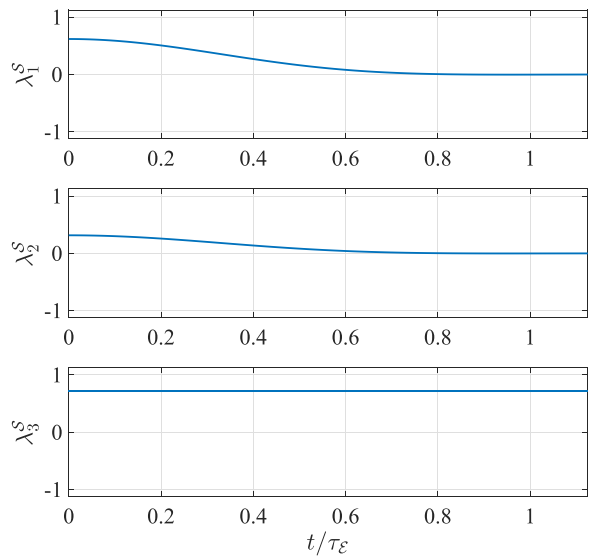


FIG. 5. Decoherence driven by interaction with an environmental shell. The same environmental configuration as in Fig. 3 is used with the same initial state. Here, however, system internal dynamics are suppressed by setting $\gamma_{\mathcal{S}} = 0$, leaving only the environmentally-driven decoherence. Only the evolution calculated using the full operator-sum representation is shown here.

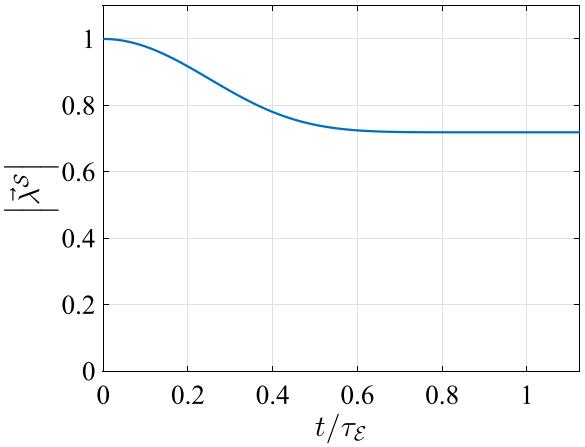


FIG. 6. Quantum coherence for the evolution of Fig. 5 as quantified by $|\vec{\lambda}^{\mathcal{S}}(t)|$. The target molecule starts with full coherence ($|\vec{\lambda}^{\mathcal{S}}(0)| = 1$) but exhibits a loss in coherence with a Gaussian time dependence as environmental interaction drives a decay in $|\lambda_1^{\mathcal{S}}(t)|$ and $|\lambda_2^{\mathcal{S}}(t)|$ asymptotically to zero. Since $\gamma_{\mathcal{S}} = 0$ here, charge tunneling is suppressed in the target molecule, and $\vec{\lambda}_3^{\mathcal{S}}(t) = \vec{\lambda}_3^{\mathcal{S}}(0)$. Thus, the asymptotic length of $\vec{\lambda}^{\mathcal{S}}(t)$ is determined by $|\lambda_3^{\mathcal{S}}(0)|$.

the $f(t)$ given in Eq. (16) determines the decay in coherence, which is Gaussian in the early time limit. Appendix B describes a linearization technique used to demonstrate the Gaussian form of $|f(t)|$.

The Gaussian time dependence of $|f(t)|$ —and thus, of $|\vec{\lambda}^{\mathcal{S}}(t)|$ also—is consistent with the illuminating result of Zurek, *et al.*, for quantum decoherence in a spin system surrounded by an environment of neighboring spin systems.[24] In both cases, a Markovian model for the environment would be insufficient to capture this time-dependence. Our work is novel in that the interaction of the target system with its environment is calculated for an explicitly modeled environment and that the emphasis here is on finding operator-sum models of decoherence.

The energy $E_o$ is a particularly effective measure of the strength of the environmental interaction because it predicts the timescale for Gaussian decoherence. The standard deviation $\sigma_t$ of $f(t)$ is inversely proportional to the environmental interaction strength $E_o$

$$\sigma_t = \frac{\hbar}{E_o}. \tag{19}$$

Figure 7 demonstrates the inverse relationship between $E_o$ and $\sigma_t$. Here, $\sigma_t$ is calculated from the early time behavior of $f(t)$, as discussed in Appendix B. On the other hand, $E_o$ is calculated directly from the Coulomb interactions between the system and the environment cells. Here, the time evolution $\vec{\lambda}^{\mathcal{S}}(t)$ was calculated from one particular initial state $\vec{\lambda}^{\mathcal{S}}(0)$ for fifty different random environments of radius $R = 1.75a$ at a given environmental population $N$. This was repeated for various population sizes $N$. In each case, $E_o$ accurately characterizes the timescale for $f(t)$ by predicting its standard deviation $\sigma_t$. Also, for a given environmental radius $R$, highly-populated environments (having larger $N$) tend to interact more intensely with the system (having higher $E_o$), driving a faster loss of coherence (characterized by a lower $\sigma_t$).

Figure 8 provides further evidence that $E_o$ characterizes the strength of the system-environment interaction and

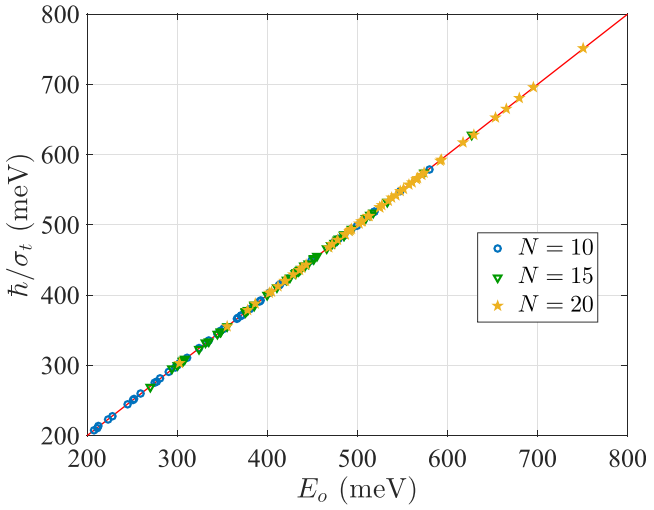


FIG. 7. The relationship between $\hbar/\sigma_t$ and $E_o$ is highly linear. Here, $\hbar/\sigma_t$ is plotted against $E_o$ for several random environmental configurations for various values of environmental population $N$. In each calculation, $a = 1$ nm and $R/a = 1.75$. In all cases, the points $(E_o, \hbar/\sigma_t)$ fall on the red line marking $E_o = \hbar/\sigma_t$.

accurately predicts the timescale for the loss of coherence. Here, $\hbar/\sigma_t$ is plotted against $E_o$ for fifty time evolutions, each with a different randomized environment of population $N = 18$ at a given environmental radius $R$. This is performed for four different environmental radii. As in Fig. 7, each $(E_o, \hbar/\sigma_t)$ point falls on the red line marking $E_o = \hbar/\sigma_t$. Environmental shells of smaller $R$ interact more strongly with the target cell and drive decoherence on a shorter timescale. This is consistent with the fact that the potential energy of Coulomb interaction is inversely proportional to $R$. Additionally, as $R$ decreases, the randomized orientation of each environmental molecule has a greater impact on the overall energetics of the system, yielding higher variation in the $E_o$ values. At large values of $R$, however, the random orientation of the environmental molecules has very little impact on the already weak (low-$E_o$) system-environmental interaction. Thus, for large $R$ values, the $(E_o, \hbar/\sigma_t)$ pairs are

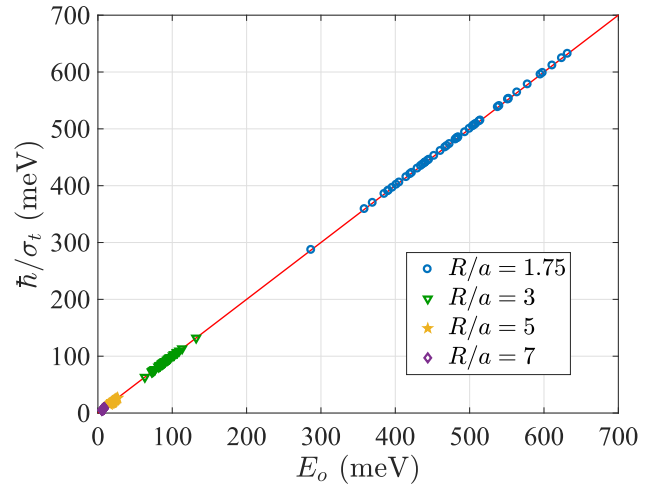


FIG. 8. The highly linear relationship between $\hbar/\sigma_t$ and $E_o$. Here, $\hbar/\sigma_t$ is plotted against $E_o$ for several random environmental configurations of population $N = 18$ at several values of environmental radius $R$. In all cases, the points $(E_o, \hbar/\sigma_t)$ fall on the red line marking $E_o = \hbar/\sigma_t$.

closely clustered near one point on the $E_o = \hbar/\sigma_t$ line at low $E_o$; on the other hand, for smaller $R$, the $(E_o, \hbar/\sigma_t)$ points exhibit more variation, but still fall on the $E_o = \hbar/\sigma_t$ line at higher values of $E_o$.

### C. A reduced operator-sum representation for the decoherence-dominated case

While the full set of Kraus operators is accurate, it also may be unwieldy. Therefore, a reduced set of Kraus operators is sought for the Gaussian decoherence in the $\gamma_S \to 0$ limit. It is well-known that a phase decay process can be modeled for a single two-state system by an operator-sum equation using only two Kraus operators[25]

$$\hat{M}_0 = \begin{bmatrix} 1 & 0 \\ 0 & \sqrt{1-T} \end{bmatrix} \quad \text{and} \quad \hat{M}_1 = \begin{bmatrix} 0 & \sqrt{T} \\ 0 & 0 \end{bmatrix}. \tag{20}$$

The desired Gaussian time dependence is obtained if

$$T = 1 - \exp\left(\frac{t}{\sigma_t}\right)^2. \tag{21}$$

Figure 9 demonstrates the use of the reduced, two-operator Kraus set defined by Eqs. (20) and (21) to approximate the exact result. The exact results are for a single time evolution of an environment of $N = 18$ molecules. This required a set of $2^{18}$ Kraus operators, each of which is a 2-by-2 matrix. For larger (but finite) $N$, the numerous environmental degrees of freedom lead to longer coherence revival times and more effectively suppress coherence in the target system. For smaller $N$, fewer environmental degrees of freedom allow more revival in quantum coherence on a shorter timescale. After the decay in coherence has reduced $f(t)$ sufficiently, slight revivals in quantum coherence slightly disrupt the Gaussian form of $f(t)$ (note: the deviation from

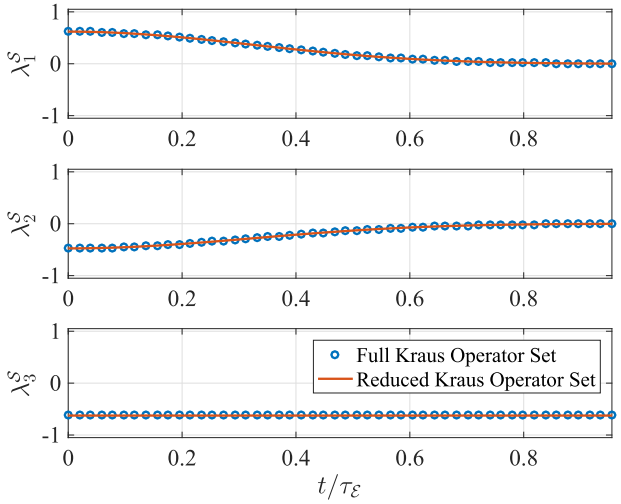


FIG. 9. Comparison of early time dynamics from a full operator-sum representation and reduced operator-sum representation. The operator-sum representation result using only the two Kraus operators (the reduced set) of Eqs. (20) and (21) very closely approximates the results of an operator-sum representation of $2^N$ Kraus operators (the full set) of the form of Eq. (17). Here, there are $N = 18$ environmental molecules, so the two-member Kraus operator set represents a significantly-reduced but highly accurate reduction of the full $2^{18}$-operator set.

Gaussian behavior is not readily observed in the plot of Fig. 9, but it is evident in the lower frame of the Appendix Fig. 10). Since the Kraus operator pair of Eq. (20) cannot model revivals in quantum coherence, this reduced operator set becomes exact in the limit of large $N$, where revivals in coherence are fully suppressed.

## V. CONCLUSIONS

Beginning with an exact model of a target double-dot QCA molecule immersed in a randomized environment of $N$ neighboring molecules, a system is established in which quantum decoherence may be studied. This is achieved by suppressing tunneling in the environmental cells, eliminating energy transfer between the target cell and its environment. In this non-dissipative limit, we select an environmental basis and calculate a full set of $2^N$ Kraus operators, which model the dynamics of the target molecule exactly in an operator-sum representation.

In the limit of electrostatic system-environment interaction dominating the internal dynamics of the target cell ($\gamma_{\mathcal{S}} \to 0$), a decay in coherence results. Specifically, this loss of coherence has a Gaussian form when coherence is measured by the length of the coherence vector $\vec{\lambda}^{\mathcal{S}}(t)$ for the target molecule.

The timescale $\sigma_t$ for the Gaussian loss of coherence is determined by $E_o$, the root-mean-square value of the energies of interaction $\{E^{\text{flip}}_{\vec{m}_p}\}$ between the target molecule and the environment in each state $|\vec{m}_p\rangle$. Here, the full, potentially-numerous set of Kraus operators can be approximated using only two operators. The approximation becomes exact in the limit of large environment population $N$, greatly alleviating the computational burden associated with this calculation.

Models of quantum decoherence and other quantum phenomena relevant in QCA operation are an important step in the realization of molecular QCA computing systems. Presently, molecular QCA remain unrealized, and the performance of candidate molecules is unknown. Models of molecular QCA can close a theoretical design loop in which candidate molecules are characterized using quantum chemistry, their performance is predicted using appropriate models, and the molecular design is altered as required to optimize performance. This can lead to vast savings in resources by avoiding the development of synthesis routes for unoptimized molecules, a task that may take years for a single candidate molecule. Such models could play a significant enabling role in the realization of high-speed, energy-efficient, molecular QCA computing devices.

## ACKNOWLEDGMENTS

This work was supported in part by the U.S. Government with support under and awarded by DoD, Air Force Office of Scientific Research, National Defense Science and Engineering Graduate (NDSEG) Fellowship, 32 CFR 168a; the National Science Foundation (NSF) under Graduate Research Fellowship Grant No. DGE-1313583; and by a research start-up grant from Baylor University. The authors acknowledge Craig Lent of the University of Notre Dame for engaging discussion.

## APPENDIX A: DERIVATION OUTLINE FOR THE FULL OPERATOR-SUM REPRESENTATION

The derivation of the full Kraus operator set begins with the solution $\hat{\rho}(t)$ to the quantum Liouville equation

$$\hat{\rho}(t) = \hat{U}(t)\hat{\rho}(0)\hat{U}^{\dagger}(t)\,. \tag{A1}$$

The initial global density matrix $\hat{\rho}(0) = \hat{\rho}_{\mathcal{S}}(0) \otimes |\mathcal{E}_0\rangle\langle\mathcal{E}_0|$ is a tensor product of a system initial state $\hat{\rho}_{\mathcal{S}}(0)$ and an environmental initial state $\hat{\rho}_{\mathcal{E}}(0) = |\mathcal{E}_0\rangle\langle\mathcal{E}_0|$. Here, $|\mathcal{E}_0\rangle$ is the state-vector representation of the initial environmental state.

It is well-known that Kraus operators are not unique but rather are basis-dependent. Therefore, we select the environmental computational basis $\{|\vec{m}_p\rangle\}$ as the basis over which we trace out the reduced density matrix $\hat{\rho}_{\mathcal{S}}(t)$ for $\mathcal{S}$ from the global density matrix $\hat{\rho}(t)$

$$\begin{aligned}\hat{\rho}_{\mathcal{S}}(t) &= \text{Tr}_{\mathcal{E}}\,\hat{\rho}(t) = \sum_{p=0}^{2^N-1}\langle\vec{m}_p|\hat{\rho}(t)|\vec{m}_p\rangle \\ &= \sum_{p=0}^{2^N-1}\langle\vec{m}_p|\hat{U}(t)\hat{\rho}_{\mathcal{S}}(0)|\mathcal{E}_0\rangle\langle\mathcal{E}_0|\hat{U}^{\dagger}(t)|\vec{m}_p\rangle.\end{aligned}$$

Here, the environment consists of $N$ two-state systems and has $2^N$ degrees of freedom. We commute $\hat{\rho}_{\mathcal{S}}$ and $|\mathcal{E}_0\rangle$ with impunity since $\hat{\rho}_{\mathcal{S}}$ acts on the Hilbert space of the system $\mathcal{S}$, but $|\mathcal{E}_0\rangle$ is of the Hilbert space of the environment

$$\hat{\rho}_{\mathcal{S}}(t) = \sum_{p=0}^{2^N-1}\langle\vec{m}_p|\hat{U}(t)|\mathcal{E}_0\rangle\hat{\rho}_{\mathcal{S}}(0)\langle\mathcal{E}_0|\hat{U}^{\dagger}(t)|\vec{m}_p\rangle\,.$$

Finally, define $\hat{K}_{\vec{m}_p}(t) \equiv \langle\vec{m}_p|\hat{U}(t)|\mathcal{E}_0\rangle$ to obtain the more compact result, the operator-sum equation

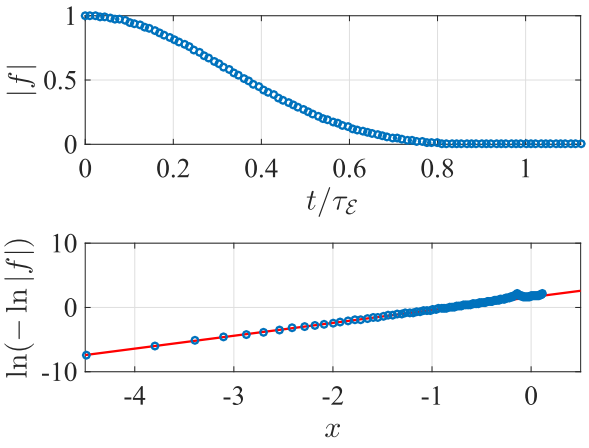


FIG. 10. The function $|f(t)|$ (upper panel) captures the time dependence of the data given in Fig. 5. In the lower panel, the linearization of Eq. (B2) is calculated and plotted so that $y = \ln(-\ln|f(t)|)$ and $x = \ln t$. A red line of slope 2 is superimposed on the data, showing that the data have a time-dependence which is very close to Gaussian, especially as $t \to 0$ (or $x$ becomes very negative). As $|f(t)| \to 0$ with increasing time, slight deviations from the Gaussian form become more evident. These deviations are due to the finite environmental population ($N < \infty$), which allows revivals in coherence on a finite timescale.

$$\hat{\rho}_{\mathcal{S}}(t) = \sum_{p=0}^{2^N-1} \hat{K}_{\vec{m}_p}(t)\hat{\rho}_{\mathcal{S}}(0)\hat{K}^{\dagger}_{\vec{m}_p}(t)\,, \tag{A2}$$

where $\hat{K}_{\vec{m}_p}(t)$ is the $p$th Kraus operator. A combination of computer and manual algebraic manipulations in the limit of suppressed charge tunneling in the environment ($\gamma_{\mathcal{E}} = 0$) was undertaken to find the form of $\hat{K}_{\vec{m}_p}(t)$. The remainder of this discussion assumes the $\gamma_{\mathcal{E}} = 0$ limit.

We can expand the environmental state $|\mathcal{E}_0\rangle$ using the computational basis states

$$|\mathcal{E}_0\rangle = \sum_{p=0}^{2^N-1} c_p|\vec{m}_p\rangle.$$

It can be shown that $\langle\vec{m}_p|\hat{U}(t)|\vec{m}_{p'}\rangle = \hat{0}$ for $p \neq p'$, thus reducing $\hat{K}_{\vec{m}_p}(t)$ to

$$\hat{K}_{\vec{m}_p}(t) = c_p\langle\vec{m}_p|\hat{U}(t)|\vec{m}_p\rangle. \tag{A3}$$

The coefficient $c_p$ can be determined under problem constraints imposed on the environmental initial state $|\mathcal{E}_0\rangle$. $|\mathcal{E}_0\rangle$ is chosen to be a direct product of $N$ charge-neutral environment cells, each having an initial state

$$|\psi_l(0)\rangle = \frac{e^{i\theta_l}}{\sqrt{2}}\left(|0_l\rangle + e^{i\phi_l}|1_l\rangle\right).$$

Thus, the environmental initial state may be written as

$$\begin{aligned}|\mathcal{E}_0\rangle &= |\psi_N(0)\rangle|\psi_{N-1}(0)\rangle\cdots|\psi_2(0)\rangle|\psi_1(0)\rangle \\ &= \frac{e^{i\Theta}}{2^{N/2}}\sum_{p=0}^{N_{\mathcal{E}}-1} e^{i\Phi_p}|\vec{m}_p\rangle\,,\end{aligned}$$

where

$$\Theta = \sum_{l=1}^{N}\theta_l\,, \quad \text{and} \quad \Phi_p = \sum_{l=1}^{N}\left[\vec{m}_p\right]_l\phi_l\,.$$

Here, $[\vec{m}_p]_l$ is the $l$th digit of the binary word $\vec{m}_p$, as in Eq. (1). Thus, $c_p$ is clearly

$$c_p = \langle\vec{m}_p|\mathcal{E}_0\rangle = 2^{-N/2}e^{i(\Theta+\Phi_p)}\,.$$

However, the phase factor $e^{i(\Theta+\Phi_p)}$ may be neglected in $\hat{K}_{\vec{m}_p}(t)$, because $\hat{K}^{\dagger}_{\vec{m}_p}(t)$ introduces the conjugate factor $e^{-i(\Theta+\Phi_p)}$, eliminating any impact the factor $e^{i(\Theta+\Phi_p)}$ might have on the time dependence of Eq. (A2).

It can be shown by a combination of computer analysis and hand analysis that

$$\begin{aligned}\langle\vec{m}_p|\hat{U}(t)|\vec{m}_p\rangle = &\frac{1}{\epsilon_{\vec{m}_p}}\left(\epsilon_{\vec{m}_p}\cos\left(\frac{\epsilon_{\vec{m}_p}t}{2\hbar}\right)\hat{I}\right. \\ &\left.+i\sin\left(\frac{\epsilon_{\vec{m}_p}t}{2\hbar}\right)\left(2\gamma_{\mathcal{S}}\hat{\sigma}_1 + E^{\text{flip}}_{\vec{m}_p}\hat{\sigma}_3\right)\right),\end{aligned}$$

with $\epsilon_{\vec{m}_p}$ and $E^{\text{flip}}_{\vec{m}_p}$ as given in Eqs. (11) and (12). Following the prescription of Eq. (A3), we multiply this by $2^{-N/2} = 1/\sqrt{N_{\mathcal{E}}}$ to account for $c_p$ (modulo the phase factor $e^{i(\Theta+\Phi_p)}$) and obtain the expression of Eq. (14) for the $p$th Kraus operator $\hat{K}_{\vec{m}_p}(t)$.

## APPENDIX B: A LINEARIZATION TECHNIQUE FOR FITTING GAUSSIAN DATA

Let a Gaussian function $g(t)$ of unit height be described by

$$g(t) = \exp\left(-\left(\frac{t-t_0}{\sqrt{2}\sigma}\right)^2\right), \tag{B1}$$

where $t_0$ is the position of the Gaussian peak, and $\sigma$ is the standard deviation of the Gaussian. A linear relationship is obtained if the natural logarithm of this function is taken twice with one intervening sign flip

$$\begin{aligned}\ln(-\ln(g(t))) &= 2\ln\left(\frac{t-t_0}{\sqrt{2}\sigma}\right) \\ &= 2\ln(t-t_0) - 2\ln\left(\sqrt{2}\sigma\right).\end{aligned} \tag{B2}$$

Thus, if a set of data $h(t)$ has a Gaussian dependence on $t$, then a plot of $y = \ln(-\ln(h))$ versus $x = \ln t$ will yield a line of slope 2. Moreover, the standard deviation $\sigma$ may be obtained from $y_0$, the $y$-intercept of the linearized data

$$\sigma = \frac{1}{\sqrt{2}}\exp\left(-\frac{y_0}{2}\right). \tag{B3}$$

We demonstrate in Fig. 10 the approximate Gaussian time dependence of the data shown in Fig. 5. The function $|f(t)|$, which determines the time dependence of $|\vec{\lambda}^{\mathcal{S}}(t)|$ for that particular evolution, is plotted in the upper panel of Fig. 10. $|f(t)|$ is linearized according to Eq. (B2) yielding the plot of $\ln(-\ln|f|)$ versus $x = \ln(t/\tau_{\mathcal{E}})$ in the lower panel. Since these transformed data are closely fitted to a line of slope 2, this time dependence is shown to be approximately Gaussian. The Gaussian fit is increasingly accurate at early times (negative $x$ with large magnitude).


[1] W. H. Zurek, Phys. Today **44**(10), 36 (1991).
[2] E. Blair and C. Lent, J. Appl. Phys. **113**, 124302 (2013).
[3] C. Lent, P. Tougaw, W. Porod, and G. Bernstein, Nanotechnology **4**, 49 (1993).
[4] P. D. Tougaw, C. S. Lent, and W. Porod, J. Appl. Phys. **74**, 3558 (1993).
[5] C. S. Lent and P. D. Tougaw, J. Appl. Phys. **74**, 6227 (1993).
[6] A. O. Orlov, I. Amlani, G. H. Bernstein, C. S. Lent, and G. L. Snider, Science **277**, 928 (1997).
[7] I. Amlani, A. O. Orlov, G. L. Snider, C. S. Lent, and G. H. Bernstein, Appl. Phys. Lett. **72**, 2179 (1998).
[8] G. L. Snider, O. Orlov, I. Amlani, G. H. Bernstein, C. S. Lent, J. L. Merz, and W. Porod, Solid-state Electron. **42**, 1355 (1998).
[9] I. Amlani, A. O. Orlov, G. Toth, G. H. Bernstein, C. S. Lent, and G. L. Snider, Science **284**, 289 (1999).
[10] A. O. Orlov, I. Amlani, G. Toth, C. S. Lent, G. H. Bernstein, and G. L. Snider, Appl. Phys. Lett. **74**, 2875 (1999).
[11] G. L. Snider, A. O. Orlov, I. Amlani, G. H. Bernstein, C. S. Lent, J. L. Merz, and W. Porod, Jpn. J. Appl. Phys., Part 1 **38**, 7227 (1999).
[12] A. O. Orlov, I. Amlani, R. K. Kummamuru, R. Ramasubramaniam, G. Toth, C. S. Lent, G. H. Bernstein, and G. L. Snider, Appl. Phys. Lett. **77**, 295 (2000).
[13] A. O. Orlov, R. K. Kummamuru, R. Ramasubramaniam, G. Toth, C. S. Lent, G. H. Bernstein, and G. L. Snider, Appl. Phys. Lett. **78**, 1625 (2001).
[14] C. Smith, S. Gardelis, A. Rushforth, R. Crook, J. Cooper, D. Ritchie, E. Linfield, Y. Jin, and M. Pepper, Superlattices Microstruct. **34**, 195 (2003).

[15]F. Perez-Martinez, I. Farrer, D. Anderson, G. A. C. Jones, D. A. Ritchie, S. J. Chorley, and C. G. Smith, Appl. Phys. Lett. **91**, 032102 (2007).
[16]M. B. Haider, J. L. Pitters, G. A. DiLabio, L. Livadaru, J. Y. Mutus, and R. A. Wolkow, Phys. Rev. Lett. **102**, 046805 (2009).
[17]C. S. Lent, P. D. Tougaw, and W. Porod, in *Workshop on Physics and Computation, PHYSCOMP'94 Proceedings* (1994), pp. 5–13.
[18]C. S. Lent, Science **288**, 1597 (2000).
[19]C. S. Lent and M. Lieberman, in *Abstracts of Papers of the American Chemical Society* (2002), Vol. 224, p. 035.
[20]M. Lieberman, S. Chellamma, Y. L. Wang, Q. L. Hang, G. Bernstein, and C. S. Lent, in *Abstracts of Papers of the American Chemical Society* (2002), Vol. 224, p. 036.
[21]K. Kraus, Ann. Phys. **64**, 311 (1971).
[22]G. Lindblad, Commun. Math. Phys. **48**, 119 (1976).
[23]G. Mahler and V. A. Weberruss, *Quantum Networks: Dynamics of Open Nanostructures*, 2nd ed. (Springer, 2008).
[24]F. Cucchietti, J. Paz, and W. Zurek, Phys. Rev. A **72**, 052113 (2005).
[25]M. Nielsen and I. Chuang, *Quantum Computation and Quantum Information*, 10th ed. (Cambridge University Press, 2011).